Editors' Suggestion

Origins of magnetic memory and strong exchange bias bordering magnetic compensation in mixed-lanthanide systems

Tyler J. Del Rose,[1,2,*] Yaroslav Mudryk,[1] Daniel Haskel,[3] Arjun K. Pathak,[4] and Vitalij K. Pecharsky[1,2]

[1]*The Ames Laboratory, U.S. Department of Energy, Iowa State University, Ames, Iowa 50011-2416, USA*

[2]*Department of Materials Science and Engineering, Iowa State University, Ames, Iowa 50011-1096, USA*

[3]*Advanced Photon Source, Argonne National Laboratory, Argonne, Illinois 60439, USA*

[4]*Department of Physics, SUNY Buffalo State, Buffalo, New York 14222, USA*

(Received 7 February 2022; accepted 5 April 2022; published 28 April 2022)

Unexpected physical phenomena resulting from the seemingly inconsequential substitutions of chemically similar lanthanide elements in the $Pr_{1-x}Gd_xScGe$ system are exploited to further the understanding of rare-earth magnetism and inform materials design. By directly probing magnetic moments of crystallographically indistinguishable Pr and Gd we solve the puzzles of how an unusual magnetic memory and strong exchange bias emerge at specific, easily predictable chemistries. Both effects are rooted in a robust antiparallel arrangement of large $4f$ magnetic moments of light and heavy lanthanides. This enables precise control of nearly zero net magnetization either opposed to, or aligned with, the external magnetic field that persists over a wide range of temperatures and fields. Further, spontaneous perturbations in the random distribution of lanthanide ions makes strong exchange bias possible in bulk single-phase compounds bordering magnetic compensation, consequently expanding the materials base beyond artificial magnetic multilayers and broadening the range of potential applications of the phenomenon.

DOI: 10.1103/PhysRevMaterials.6.044413

I. INTRODUCTION

Lanthanides have some of the highest atomic magnetic moments known in nature that vary systematically across the series of the 15 chemically similar $4f$ elements. Together with Y and Sc, they make up the rare-earth series, forming numerous families of compounds with other metals and metalloids, many of which have already become or may soon become the foundation of advanced materials indispensable for modern technology. Among those are hard magnets for energy generation and conversion [1,2], compounds that exhibit strong magnetocaloric effects for solid-state heat pumping [3,4], materials for quantum information and quantum computing [5,6], high-temperature superconductors for energy transmission and use [7], and magnetic materials for next-generation data storage [8,9]. To fulfill the promise of future innovation that takes advantage of important and/or unusual properties of $4f$ materials, systematic examination of their composition-structure-property relationships is required, including addressing known challenges [10,11]. Some of the challenges, real and perceived, include difficulties of synthesis due to high-temperature volatility of Sm, Eu, and a few other lanthanides, reactivity of light lanthanides at ambient conditions, potential for local chemical inhomogeneities that are difficult to eliminate when two or more of the lanthanides are present, underdeveloped theory related to proper modeling of $4f$ states, strong influence and variability of crystalline electric fields, and complexity of magnetic structures. At the same time, those challenges present clear opportunities to establish the missing science of how fundamentally and practically important phenomena emerge, with new knowledge to be unearthed in almost every rare-earth system.

Among the vast array of known intermetallic compounds, the equiatomic RTX family (R = rare earth, T = transition metal, and X = p-block element) constitutes a relatively well-studied subgroup of rare-earth materials. The RTX series holds more than 5600 [12] unique ternary combinations and nearly an infinite number of pseudobinary, multinary variants considering ease of feasible substitutions on the R as well as T and X sites. Members of the family have been shown to crystallize in a multitude of structures, exhibiting physical phenomena that can be clearly related to their crystallography, as summarized in a number of reviews [13–19]. Specifically, RScGe compounds crystallizing in a layered CeScSi-type structure [20] are an ideal subgroup to examine the interactions between differing lanthanides in detail. Here, Ge atoms separate corrugated R layers from flat Sc sheets while mirror symmetry doubles its unit cell along the c axis and differentiates it from the closely related CeFeSi-type structure. Despite the relative crystallographic simplicity, CeScSi/CeFeSi-type structures show a plethora of interesting physical properties. For example, a neutron diffraction study revealed that on cooling PrScGe undergoes a paramagnetic (PM) to antiferromagnetic (AFM) transition at 140 K, followed by an AFM to ferrimagnetic (FiM) transition at 88 K, and a spin reorientation transition at 80 K [21]. GdScGe, on the other hand, becomes ferromagnetic (FM) at 350 K, well above the Curie temperature, T_C = 293 K, of its only nominally magnetic element, Gd [22]. Furthermore, negative magnetization and large

*Corresponding author: tdelrose@iastate.edu

exchange bias have been reported in $Sm_{1-x}Nd_xScGe$ and $Nd_{1-x}Gd_xScGe$ [23].

An easily predictable, nearly ideal pseudobinary solid solution of the aforementioned germanides exemplifies the phrase "complexity is opportunity" by adding interactions between the heavy ($J = L + S$, where L, S, and J are, respectively, the orbital, spin, and total angular momentum quantum numbers) and light ($J = L-S$) lanthanides as well as inherent chemical inhomogeneities, likely to be present at the nanoscale in real materials where Pr and Gd atoms are statistically mixed on the same crystallographic site [8,24]. Additional complexity may arise from the rare-earth element Sc that could be classified as a nonmagnetic transition metal, playing the role of such in RScX, but it may also partially substitute heavy lanthanide atoms, such as Gd [21,25–28].

In this work, we make use of the opportunity and uncover the science underpinning the unusual physical properties recently reported in $Pr_{0.75}Gd_{0.25}ScGe$, such as magnetic compensation and peculiar magnetic memory effects [8], by scrutinizing this and other $Pr_{1-x}Gd_xScGe$ compositions. Namely, we examine electronic and thermal transport properties, relating the latter to anomalous lattice expansion, and resolve the outstanding challenge of confirming the origin of magnetic compensation by directly probing the mutual orientations of lanthanide magnetic moments using x-ray magnetic circular dichroism. We also show how magnetic memory is a direct consequence of the magnetic compensation, and how the presence of chemical inhomogeneities results in exceptionally strong exchange bias of admixed, magnetically compensated lanthanide systems.

II. EXPERIMENT

A total of seven $Pr_{1-x}Gd_xScGe$ samples with $x = 0$, 0.1, 0.25, 0.35, 0.5, 0.6, and 0.75 were arc melted using stoichiometric amounts of the constituent elements, flipping each button 4–5 times during the arc melting process. All rare-earth elements were acquired from the Materials Preparation Center at Ames Laboratory and had purities of 99.9+ wt % (99.3+ at. %) with respect to all other elements in the periodic table. Germanium was purchased from Meldford Metals and was at least 99.99 wt % pure. All elements were from the same batch except for the Gd used in the $x = 0.1$ and $x = 0.25$ samples (the difference between the Gd metal batches constituted a slightly higher/lower O and Al impurity content; see Ref. [8] for details). Once in polycrystalline ingot form, the samples were wrapped in a Ta foil, sealed in a quartz tube under a partial helium atmosphere, and annealed with the following temperature profile: (1) quickly ramped up to 550 °C and held for 1 day; (2) from 550 °C quickly ramped to 950 °C and held for 2–3 weeks; and (3) the furnace was turned off to allow samples to slowly cool to room temperature.

Initial verification of crystal structures and phase purities of all samples, and temperature-dependent examination of the $x = 0.6$ sample were achieved with powder x-ray diffraction (PXRD) using a modified Rigaku TTRAX system, equipped with a low-temperature attachment, using Mo $K\alpha$ radiation [29]. Additionally, PXRD patterns of all samples were collected at the 11-BM beamline of the Advanced Photon Source (APS) at Argonne National Laboratory (ANL) with $\lambda = 0.457\,897$ Å using rapid-access mail-in service. Structural parameters were obtained through Rietveld refinements using GSAS-II [30].

Microstructures were visualized and elemental analyses were performed using an FEI Teneo scanning electron microscope (SEM) equipped with an Oxford Instruments Aztec energy dispersive spectroscopy (EDS) system. Heat capacity, magnetic, and transport properties were measured as functions of temperature and applied magnetic fields using a physical property measurement system (PPMS, Quantum Design, Inc.). Additionally, some magnetic measurements were carried out in a superconducting quantum interference device (SQUID) magnetometer (MPMS XL-7, Quantum Design, Inc.).

X-ray magnetic circular dichroism (XMCD) measurements were carried out at beamline 4-ID-D of the Advanced Photon Source at Argonne National Laboratory (APS-ANL) on powder samples with $x = 0$, 0.25, and 0.5 compositions, with specimens optimized for transmission measurements. Circularly polarized x rays of opposite helicity were generated using a 180-μm-thick diamond phase plate [31]. The XMCD data were collected in helicity switching mode with fixed magnetic field direction, whereby helicity is modulated at 13.1 Hz and the related modulation in the absorption coefficient is measured with a phase lock-in amplifier [32]. A superconducting magnet with a variable temperature insert was used for measurements in the 1.75–220 K range. Data were collected across Gd-L_3 (7.2428 keV) and Pr-L_2 (6.4404 keV) absorption edges. All samples were cooled in a 1 kOe field applied parallel to the incident beam.

III. RESULTS AND DISCUSSION

A. Crystallography and microstructure

The high-resolution synchrotron data from Advanced Photon Source (APS) were used for full-profile Rietveld refinements. All studied compounds are isostructural and adopt the layered CeScSi-type structure (space group $I4/mmm$) reported by Bodak *et al.* [20]. All refinements converged at $R_{wp} \leqslant 9\%$, $R_{F^2} \leqslant 3\%$. A slight preferred orientation was detected and accounted for during the refinements using the spherical harmonics approximation with four independent parameters. All refined powder x-ray diffraction (PXRD) data sets are shown in Figs. S1 and S2 of the Supplemental Material (SM) [33]. A majority of the samples are single phase, however, APS PXRD and electron microscopy showed a small amount of $(Sc, Pr, Gd)_5Ge_3$ in the $x = 0.6$ sample that was undetectable in the standard laboratory PXRD. Scanning electron microscopy (SEM) image analysis estimates this impurity to be 0.6 vol %. Due to the low concentration, the impurity is not expected to introduce any notable property changes, and thus will not be further discussed in this work. A list of refined structural parameters can be found in Table I for all samples studied here; the values for $x = 1$ are taken from Guillou *et al.* and references therein [22].

The $x = 0.25$ sample displays obvious asymmetry in the (00l) peaks, most notably at high l values (see Fig. S2 of the SM [33]). Other Bragg peaks, those with $l \gg h$ and k, show weaker, but still noticeable asymmetry. This, together

TABLE I. Rietveld-refined crystallographic parameters of $Pr_{1-x}Gd_xScGe$. Values for $x = 1$ are taken from Guillou *et al.* [22]. The least squares standard deviations are shown in parentheses.

X	a	c	V (a^2c)	Z (Ln)	Z (Ge)
0	4.330 00(3)	15.895 03(8)	298.012(4)	0.323 42(1)	0.122 65(2)
0.1	4.328 14(2)	15.878 91(6)	297.456(3)	0.323 53(1)	0.123 17(2)
0.25	4.315 78(2)	15.826 24(6)	295.779(3)	0.323 40(1)	0.123 70(1)
0.35	4.310 84(2)	15.801 13(5)	294.637(3)	0.323 43(1)	0.124 23(1)
0.5	4.300 83(2)	15.757 78(6)	291.473(3)	0.323 31(1)	0.124 73(2)
0.6	4.288 57(2)	15.721 48(6)	289.147(3)	0.323 39(1)	0.124 74(2)
0.75	4.279 27(1)	15.676 00(2)	287.0609(7)	0.323 08(1)	0.125 44(1)
1	4.2590(5)	15.598(1)	282.93(7)	0.322 83(6)	0.1265(1)

with the fact that the asymmetry remains minor, given the data collection geometry and high resolution, leads us to the conclusion that the crystal structure of $x = 0.25$ is the same as all other samples, but some segregation of Pr and Gd occurs at the nanoscale. We also note that Rietveld fits of all Gd-containing samples showed slight improvements to R_{wp} when refined with an additional 2% Gd on the Sc site. This is consistent with previous reports of off stoichiometry [34,35]. However, one must be careful as an addition of 2% Gd to the Sc site is minuscule, would be hard to tell if it is truly intrinsic to the samples, and given the as-weighed stoichiometry, 2% of Sc would be expected to substitute Gd on the R site. Furthermore, since PXRD data give an average unit cell, the presence of local distortions produced by minor compositional inhomogeneities across nanoscale regions in real materials is feasible.

Compositional dependence of interatomic distances, shown in Fig. 1(b), tends to follow the lattice parameters, baring the Ge-Ge distances along the c axis. From this, as Gd substitutes Pr, the corrugated rare-earth layers contract along the c axis and move closer together. This structural feature may influence magnetism—according

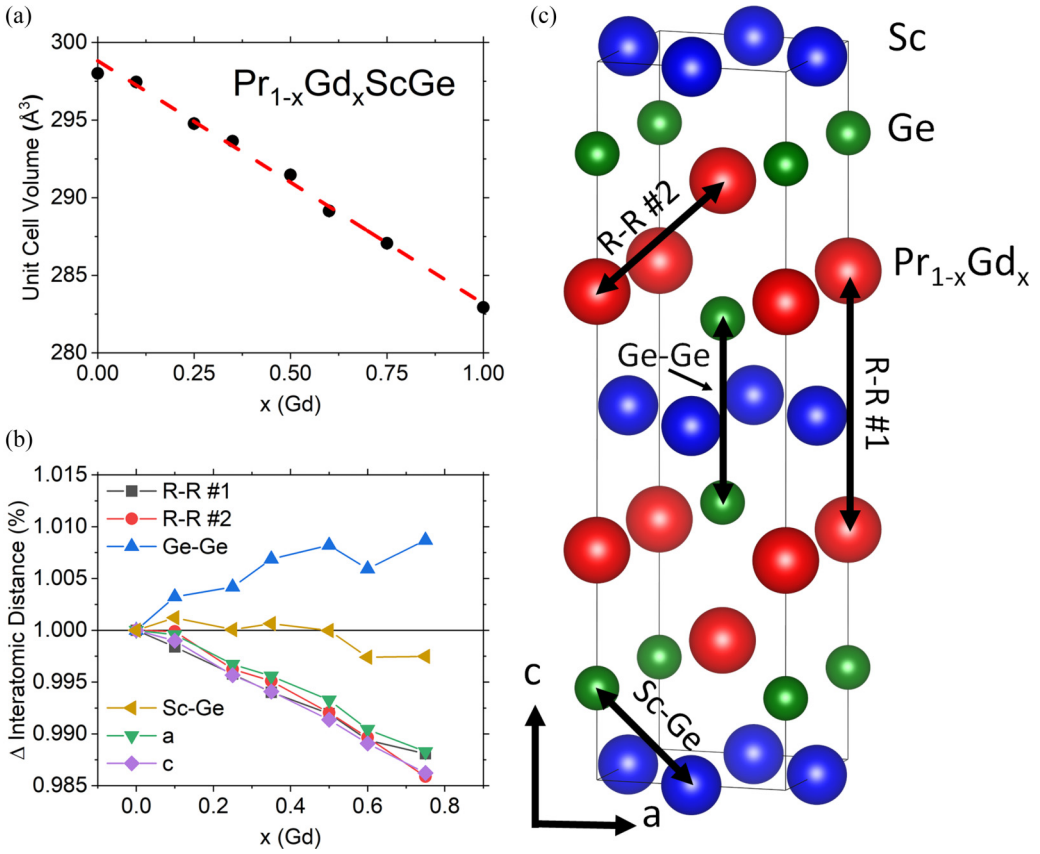

FIG. 1. Rietveld refinement results of $Pr_{1-x}Gd_xScGe$ at room temperature. (a) Unit cell volume of $Pr_{1-x}Gd_xScGe$ as a function of Gd concentration (the $x = 1$ point is from Guillou *et al.* [22]). (b) Relative changes in the nearest-neighbor interatomic distances as functions of Gd concentration. The relative changes of lattice parameters a and c are plotted for comparison. (c) Depiction of the unit cell and interatomic distances shown in (b).

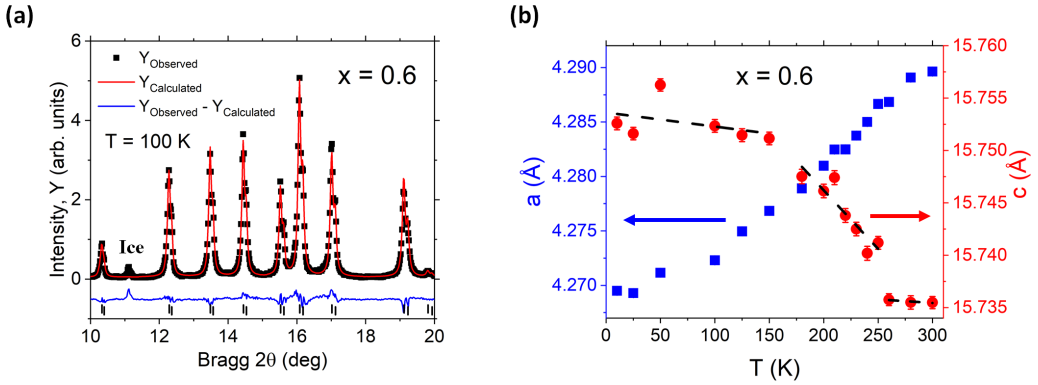

FIG. 2. Rietveld refinement results of the $x = 0.6$ sample with respect to temperature. (a) Rietveld fit of the low temperature ($T = 100$ K) PXRD data for $x = 0.6$ with only the $10^\circ \leqslant 2\theta \leqslant 20^\circ$ region shown for clarity, and (b) lattice parameters as functions of temperature. The Bragg peaks of a minor (Pr, Gd, Sc)$_5$Ge$_3$ impurity phase could not be seen in a laboratory PXRD. The Bragg peak near $2\theta = 11^\circ$ in (a) is due to a small amount of the cubic polymorph of ice forming [36], common for this system [37]. The dashed lines in (b) are linear fits of the c parameter highlighting three distinct regions.

to the Ruderman-Kittel-Kasuya-Yosida (RKKY) theory the strength of the lanthanide exchange interaction is an exponentially decaying oscillating function of 4f-element spacing. Additionally, Ge-Sc interatomic distances remain nearly invariant with respect to changes in the unit cell dimensions despite a gradual reduction of both a and c, and cell volume.

SEM and energy dispersive spectroscopy (EDS) data confirm the single-phase nature of all synthesized materials (see SM Fig. S3 [33]), except for some surface oxidation during polishing and the presence of a minor impurity phase in $x = 0.6$. All materials are extremely brittle, hence micropores and microcracks are abundant, and are likely a result of polishing as well. Furthermore, the $x = 0.25$ sample was the only sample to chemically etch when polished with water-based colloidal silica despite the same crystal structure and chemical makeup analogous to the entire series. In light of this, all SEM images (see Fig. S3, SM [33]) are from samples polished with 1-μm diamond paste.

A low-temperature PXRD study, the results of which are illustrated in Fig. 2(a), was performed on the $x = 0.6$ sample using a laboratory PXRD setup [29] between 10 and 300 K in zero magnetic field. The a ($= b$) lattice parameter increases fairly linearly during heating over the measured range [Fig. 2(b)]. The c parameter, on the other hand, behaves unexpectedly. In addition to thermal contraction instead of thermal expansion along the longest cell dimension as temperature increases, c(T) has three distinct regions: $0\,\text{K} \leqslant T \leqslant 150$ K (slowly decreasing), $150\,\text{K} \leqslant T \leqslant 260$ K (rapidly falling), and $T \geqslant 260$ K (nearly constant). The scatter of the data is within 2–3 standard deviations, but the rapid drop of c between 150 and 260 K is intrinsic. The upper-temperature limit of this region happens to coincide with the global magnetic ordering temperature, but the anomalous thermal expansion is not believed to be exclusively a result of spontaneous striction (see Sec. III B for more details). Except for the rapid contraction along c, no other structural changes can be detected, and the PXRD pattern depicted in Fig. 2(a) is characteristic of the same CeScSi-type structure stable at $T = 100$ K, as well as at any other temperature between 10 and 300 K.

B. Heat capacity and electronic and thermal transport

Heat capacity measured in zero magnetic field for $x = 0.25$ (Fig. S4, SM [33]) shows a second-order phase transition anomaly with a maximum at 183 K. Fitting of the low-temperature data using the Debye model ($C_P \propto T^3$) for the lattice contribution and $C_P \propto T$ for the electronic contribution, modified to include nuclear heat capacity of Pr ($C_P \propto T^{-2}$), results in the Debye temperature (θ_D) of 251 K. This is in reasonable agreement with the values reported for GdScGe, CeScGe, and CeTiGe compounds [22,39,40]. It is worth noting that the large nuclear contributions resulted in unrealistic electronic contribution ($C_P \propto T$) to heat capacity.

Thermal conductivities, $\kappa_T(\text{T}) = \kappa_L(\text{T}) + \kappa_e(\text{T})$, where κ_T, κ_L, and κ_e are, respectively, total, lattice, and electronic conductivities, of $x = 0.25$ and $x = 0.6$ materials measured as functions of temperature in 0 and 10 kOe magnetic fields, are shown in Figs. 3(a) and 3(b). The electronic contributions were calculated from $\rho(T)$ data (not shown but measured concurrently [38]) using the Wiedemann-Franz law: $k_e = L_0 T \rho^{-1}$, where ρ is the DC electrical resistivity and $L_0 = 2.45 \times 10^{-8}\,\text{W}\,\Omega\,\text{K}^{-2}$ is the Lorentz number. The initial strong increases in $\kappa_T(T)$ at low temperatures correspond to the rapidly increasing number of phonons and rising kinetic energy of electrons, while the local maxima at low temperatures signify scattering due to the increased number of phonon-phonon and phonon-electron interactions. The behaviors of both the electronic and lattice contribution are not uncommon for a metallic material, baring anomalous slope changes in $\kappa_T(T)$ near 170 and 240 K for $x = 0.25$, and near 200 and 250 K for $x = 0.6$.

The anomalous slope changes do not fully correspond with spontaneous striction as $x = 0.25$ orders magnetically at 184 K, near the lower temperature (170 K) anomaly in $\kappa_T(T)$, and $x = 0.6$ orders at 270 K, above the higher temperature (250 K) slope change. However, the slope changes in $x = 0.6$ can be related to the corresponding anomalies in lattice expansion along the c axis revealed by temperature-dependent PXRD, depicted in Fig. 2(b). These anomalies are not seen in $\kappa_e(T)$, implying electrons are much less susceptible to the small volume changes than phonons. Additionally, applied

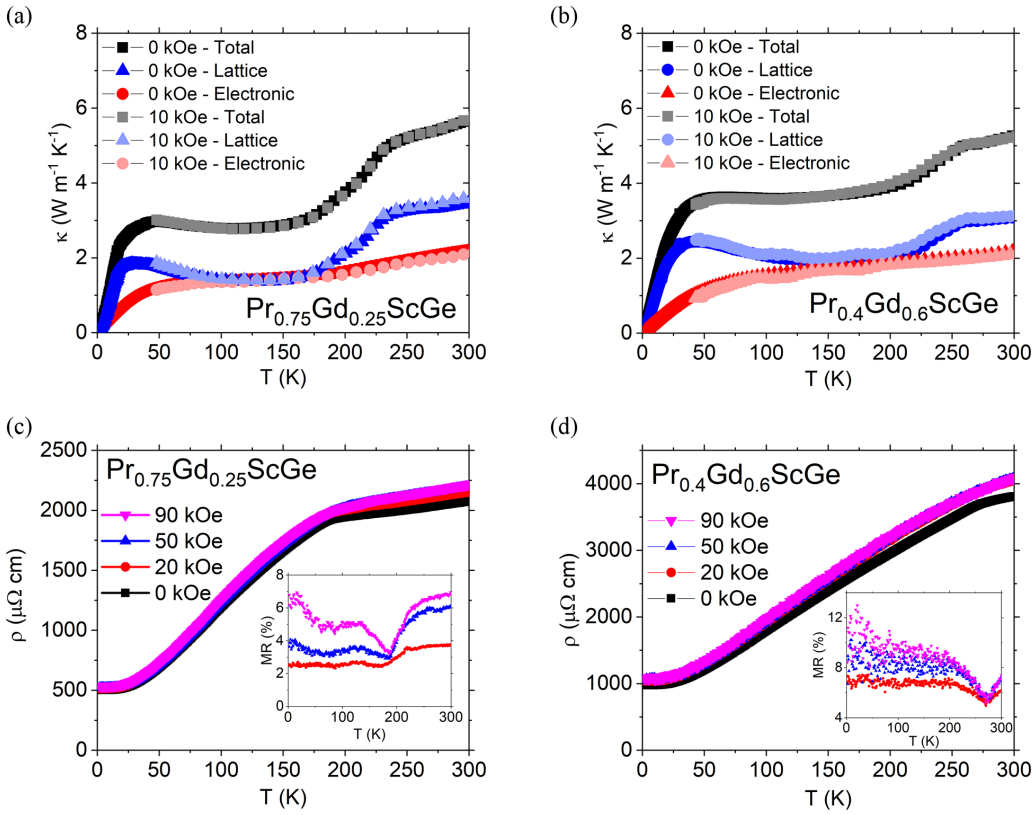

FIG. 3. Transport properties of $Pr_{0.75}Gd_{0.25}ScGe$ and $Pr_{0.4}Gd_{0.6}ScGe$. Thermal conductivity of (a) $x = 0.25$ and (b) $x = 0.6$ samples measured in 0 and 10 kOe fields during heating. The electronic contribution is estimated using the Weidemann-Franz law and electrical resistivity measured concurrently (not shown [38]). Electrical resistivity of (c) $x = 0.25$ and (d) $x = 0.6$ in 0, 20, 50, and 90 kOe fields. The insets depict magnetoresistance.

fields have little to no effect on the phononic contributions and the observed minor change in the electronic contribution with applied field is most likely due to cracks forming during thermal cycling.

Figures 3(c) and 3(d) depict the electrical resistivities measured as functions of temperature in different magnetic fields for the $x = 0.25$ and $x = 0.6$ samples. The residual resistivity ratios, RRR $\cong$ 4, are relatively low, reflective of the considerable contributions from carrier scattering on defects such as grain boundaries and microcracks naturally present in these extremely brittle materials. The resistivities show metallic character with nearly temperature-independent behaviors at $T \leqslant 25$ K, typically caused by defect dominated scattering. Slope changes occur near the corresponding T_Cs, marking the second-order magnetic phase transitions in both materials. The resistivities measured at different applied fields show minimal qualitative changes in the electronic transport behavior. Magnetoresistances (MRs) are weak and anomalous near T_Cs [insets in Figs. 3(c) and 3(d)]. The shallow minima in MRs extend over large temperature ranges indicative of the second-order nature of the magnetic transitions. The MR minima correlate very well with T_Cs found from magnetization.

C. Magnetic properties

The magnetic behaviors of the $Pr_{1-x}Gd_xScGe$ compounds are dominated by the $4f$ electrons of lanthanides, Gd and Pr, and thus follow the RKKY model of indirect exchange interactions [41–44]. However, substitution of Gd is not a trivial matter as saturation magnetization does not monotonously increase with increasing the concentration of Gd—the element with a higher magnetic moment—but instead, the addition of Gd initially decreases the saturation magnetization (Fig. 4).

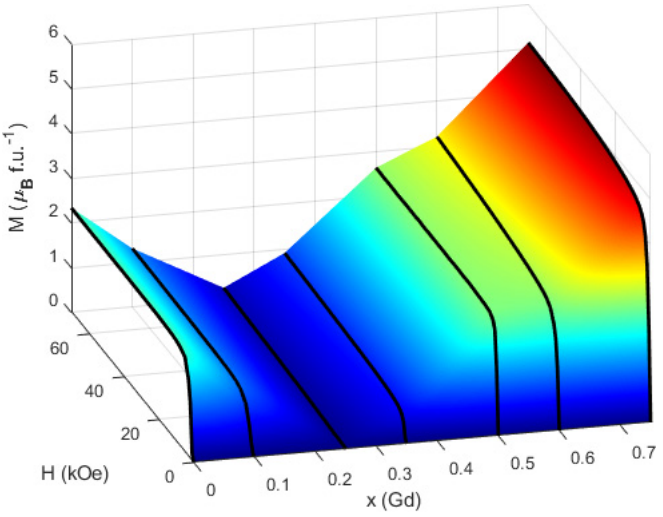

FIG. 4. Evolution of magnetization, measured as function of magnetic field and change in x(Gd) at $T = 2$ K. The black contour lines indicate measured data and the blue → green → red color scale indicates increasing magnetization.

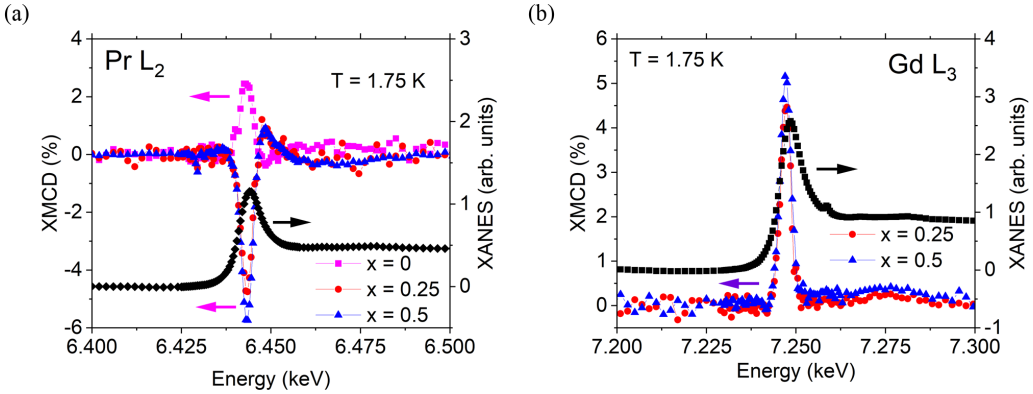

FIG. 5. XMCD and x-ray absorption near edge structure (XANES) of the (a) Pr-L_2 edge in $x = 0$, 0.25, and 0.5 and (b) Gd-L_3 edge in $x = 0.25$ and 0.5. A positive (negative) XMCD signal at Pr-L_2 (Gd-L_3) edges corresponds to Pr (Gd) magnetization having a projection along the applied field direction. The L_3 and L_2 XMCD data are normalized to isotropic absorption jump of 1 and 0.5, respectively.

When the concentration of Gd reaches and exceeds 25%, the saturation magnetization begins to rise. Intuitively, this should happen when heavy and light lanthanides are mixed on the same site: because they are also early transition metals, their induced $5d$ moments and, consequently, $4f$ spin moments should be parallel. Orbital $4f$ moments are, however, either antiparallel, as in light lanthanides, or parallel, as in heavy lanthanides, to their spin moments ($J = L \pm S$), and since generally $L \geqslant S$, the magnetic moments of light lanthanides are expected to couple antiparallel with those of the heavy. Although this has been previously assumed for other rare-earth systems, for example, admixed rare-earth dialuminides [45–49], explicit experimental confirmation on a microscopic level has not yet been demonstrated.

Isothermal dependencies of magnetization (Fig. 4) indicate no spin flips in any of the mixed-lanthanide materials in fields as high as 140 kOe (not shown, but see Del Rose *et al.* [8]), suggesting a strong antiparallel coupling between the Gd ($L = 0$, $S = 7/2$, $J = 7/2$) and Pr ($L = 5$, $S = 2/2$, $J = 4$) moments. Additionally, $x = 0$ and 0.5 are the only compositions to clearly reach saturation at $H = 70$ kOe, however, the magnetization of the other four samples (excluding $x = 0.25$) is close to saturation, likely indicating minor canting between the magnetic moments of Gd and Pr.

Direct experimental evidence of antiparallel alignment between Gd and Pr moments has been obtained from x-ray magnetic circular dichroism (XMCD) measurements (Fig. 5) that provide element-specific information about magnetic moment orientation relative to an applied magnetic field. In a pure PrScGe ($x = 0$), the Pr moment has a net projection along the magnetic field direction, but as Gd replaces Pr, the moment of the latter opposes the applied magnetic field when $x \geqslant 0.25$ as illustrated in Fig. 5(a). Considering the difference between the localized magnetic moments of Pr and Gd, for Gd concentrations smaller than $x = 0.25$, Pr moment dominates and is expected to orient parallel to the applied field, thus minimizing the Zeeman energy. In fact, using the ordered moments of GdScGe and PrScGe (respectively 7.1 μ_B reported in Guillou *et al.* [22] and 2.35 μ_B; see below) determined from $M_{H=70\,\mathrm{kOe}}$, a simple linear combination of the two predicts the composition at which full magnetic compensation occurs as $x = 0.24$, in agreement with the XMCD and magnetometry data. Furthermore, keeping in mind that Zeeman energy should be minimized, the fully compensated composition also signifies the boundary between the Gd dominant and Pr dominant compositions, in terms of which lanthanide has a net moment along the field direction. It is worth noting that the experimentally determined Pr moments in this series of compounds are much lower than the theoretically expected $g\sqrt{J(J+1)} = 3.58\,\mu_B$/Pr and $gJ = 3.2\,\mu_B$/Pr, pointing towards a large crystal field splitting as the main reason for the lower Pr moment in accordance with previous reports [25].

The increase in the Pr-L_2 XMCD signal for $x \neq 0$ [Fig. 5(a)] indicates a more collinear alignment of the Pr magnetic moments with field. The minor but obvious increases in Pr-L_2 [Fig. 5(a)] and Gd-L_3 [Fig. 5(b)] XMCD signals from $x = 0.25$ to $x = 0.5$ also indicate that projections of the corresponding magnetic moments are more in line with the applied field. Furthermore, the magnitude of the Gd-L_3 peak is slightly lower than what is expected of Gd moments coinciding with the applied field, indicative of minor canting [50].

The bifurcation between $M_{H=70\,\mathrm{kOe}}$ (negative slope) and ρ_{eff} (positive slope) for $x \leqslant 0.25$ [Fig. 6(a) and Table II] further exemplifies the antiparallel orientation of the Gd and Pr moments in the ordered state. Noting that this magnetic ordering neither constitutes nor represents a classical ferrimagnetic (FiM) system as the Gd and Pr ions carrying different magnetic moments share the same lattice site, nor does this represent a spin wave as the substitution is a nearly random statistical mixture, the title materials will be referred to as ferrimagnets throughout this work. AC magnetic susceptibility measured for $x = 0.25$ over the temperature range 2–300 K [8] shows no frequency dependence, and thus the formation of a spin-glass state is unlikely as well.

The $x = 0.1$ sample has the same T_C as $x = 0$ despite having drastically different Weiss temperature (θ_P), $M_{H=70\,\mathrm{kOe}}$, and ρ_{eff} values (Table II). With a 90% probability for any given lanthanide atom to be Pr at this composition, the probability that all four lanthanide atoms are Pr in an average $Pr_{0.9}Gd_{0.1}ScGe$ unit cell is $0.9^4 = 0.66$. Hence 66% of the cells are exclusively PrScGe. However, when a given unit cell accommodates Gd, its magnetic moment still orients an-

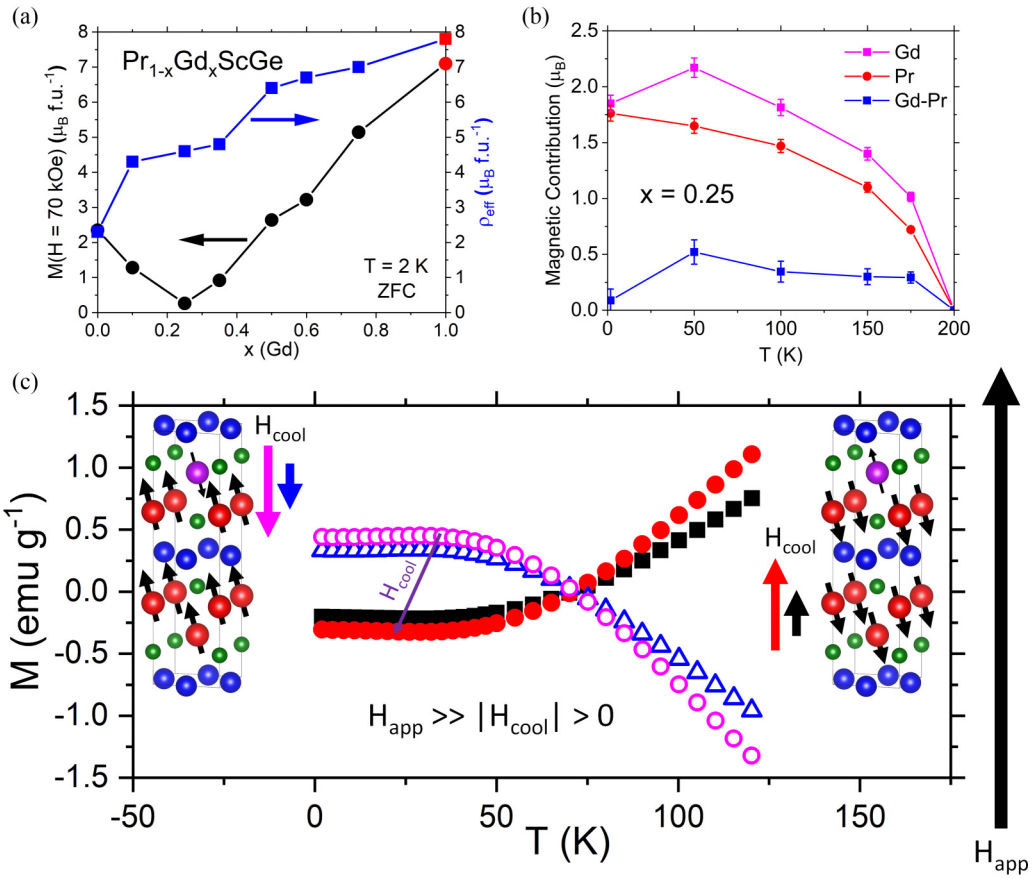

FIG. 6. (a) Effective magnetic moment and magnetization at $H = 70$ kOe plotted as functions of gadolinium concentration. The red points at $x = 1$ are taken from Guillou *et al.* [22]. (b) Depiction of the change in XMCD signal with respect to temperature normalized to XMCD signals at $T = 1.75$ K. (c) The unusual magnetic effects this work addresses, that is, negative magnetization and magnetic memory effects in $Pr_{0.75}Gd_{0.25}ScGe$ (full data sets are in Ref. [8]). H_{cool} is the field applied prior to measurement, on cooling (ranging −20 to 20 Oe), and H_{app} is the field applied while measuring (0.1 kOe, always positive).

tiparallel to that of Pr as evident from $M_{H=70\,kOe}$. This could indicate a rather interesting magnetic structure as Pr in ternary PrScGe is known to split into multiple, differently degenerate $4f$ states with different magnetic moments that orient antiparallel [21], and minor Gd additions could cause the complex ferrimagnetic magnetic structure, intrinsic to pure PrScGe, to become frustrated.

The negative magnetization and atypical magnetic memory effects earlier reported for $Pr_{0.75}Gd_{0.25}ScGe$ in Del Rose *et al.* [8] [Fig. 6(c)] are a result of the nearly zero observed net magnetic moment and weak applied magnetic fields. Small, trapped fields intrinsic to the superconducting magnets used in SQUID devices generally oppose the previously set field [52], initially polarizing the Gd moments parallel and the Pr mo-

TABLE II. Magnetic parameters for $Pr_{1-x}Gd_xScGe$. T_Cs are assigned as the minima in dM/dT, and θ_P and p_{eff} are obtained by fitting $\chi^{-1}(T)$ to the Curie-Weiss law. T_C and $M_{H=70\,kOe}$ for $x = 1$ are taken from Guillou *et al.* [22], while θ_P and p_{eff} are from Ivanova *et al.* [51]. The value of p_{eff} marked with an asterisk represents an average of two samples prepared from different batches of the Gd metal with minor differences in the impurity concentrations (see Ref. [8] for details on the effects of Gd impurities).

x (Gd)	T_C or T_N (K)	θ_P (K)	$M_{H=70\,kOe}$ (μ_B/f.u.)	p_{eff} (μ_B/f.u.)
0	140	125	2.35	2.3
0.1	140	15.6	1.28	4.3
0.25	186	135	0.26	4.6*
0.35	211	194	0.92	4.8
0.5	246	236	2.64	6.4
0.6	270	275	3.22	6.7
0.75	306	324	5.14	7.0
1	352	332	7.4	7.8

ments antiparallel to those trapped fields for $x \geqslant 0.25$ and vice versa for $x<0.25$. As temperature decreases across and below the Curie temperature, the Gd and Pr moments are "frozen" in place, so when a magnetic field smaller than the coercivity but opposing the trapped field is applied at the lowest temperature, the Gd moment remains oriented antiparallel and Pr parallel to the new applied field. This results in negative magnetizations when $x = 0.25$.

Additionally, as depicted in Fig. 6(b), the localized lanthanide moments develop nonuniformly with temperature and the competing Gd and Pr magnetic sublattices are expected to create a near zero net magnetic moment at all temperatures for at least $x = 0.25$. Even though Fig. 6(b) shows positive net magnetization at all temperatures, it assumes perfectly antiparallel Gd and Pr moments that are collinear with the applied magnetic field. Minor canting in either the Pr or Gd sublattices, or both, with respect to the applied field or slight changes to their collinear alignment with each other, which has been suggested previously in this work, could cause the flip between negative and positive magnetization, as shown in Fig. 6(c). Furthermore, by controlling the field, that is, by setting weak positive or negative bias fields during cooling to override the trapped fields, the initial Gd and Pr magnetic moment orientations can be flipped, causing tunable positive and negative temperature dependent magnetization regions, as depicted in Fig. 6(c).

Spontaneous exchange bias (exchange bias when cooled in zero magnetic field) was observed in $Pr_{0.75}Gd_{0.25}ScGe$ [8] as well as with other single-phase, admixed-lanthanide systems near their fully compensated compositions, for example, in $Nd_{0.75}Ho_{0.25}Al_2$ and $Sm_{0.94}Gd_{0.06}ScGe$ [23,49]. Previously it has been suggested that self-inclusions of differing magnetic structures, usually caused by metamagnetic transitions, could be an underlying cause of the spontaneous exchange bias in single phase materials [24,53,54]. However, no metamagnetic behavior is observed in any of those compounds (also refer to Fig. 4).

Instead, we propose that inhomogeneities inherent to the lanthanide chemical disorder result in exchange bias in this, and, consequentially, other substituted and magnetically ordered, nearly fully compensated lanthanide systems. In the case of $Pr_{0.75}Gd_{0.25}ScGe$, imperfections in the local chemical disorder, as discussed in Sec. III A, could result in regions of slightly lower (or higher) Gd concentrations. Usually, this would have minute consequences, as the properties of a region of slightly lower (higher) Gd concentration would be averaged out in macroscopic properties (i.e., magnetization and transport). However, $x = 0.25$ is uniquely situated on the border between a Gd and Pr dominant system, in terms of magnetic ordering direction. Thus, it is conceivable that $x = 0.25$ has both Pr dominant (inclusions that average $x<0.25$) and Gd dominant (bulk) regions. The interfaces between these regions would ensure the magnetic pinning necessary to produce exchange bias, as schematically illustrated in Fig. 7.

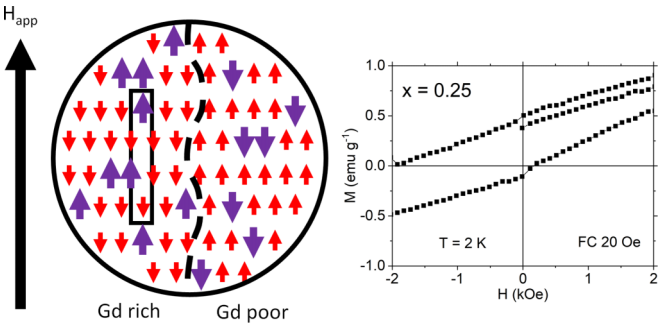

FIG. 7. Proposed mechanism (left) for producing exchange bias (right) in single-phase $Pr_{0.75}Gd_{0.25}ScGe$. The smaller, red, and larger, purple, arrows represent Pr and Gd magnetic moments, respectively, while the black, dashed line illustrates the boundary between the Gd-rich (left) and Gd-poor (right) regions. The rectangular box represents a unit cell. For a full data set illustrating the exchange bias see Ref. [8].

IV. CONCLUSIONS

Synchrotron PXRD and SEM verifies that all studied $Pr_{1-x}Gd_xScGe$ samples are single phase [except $x = 0.6$ for which SEM shows a minor, 0.6 vol % impurity of $(Sc, Pr, Gd)_5Ge_3$]. When $x = 0.25$, asymmetry in the (00ℓ) Bragg reflections is noticeably greater when compared to other isostructural members with different x, reflecting local inhomogeneity in Pr and Gd distribution. Low-temperature PXRD of $x = 0.6$ unveils anomalous anisotropic lattice expansion that correlates with anomalies in lattice thermal conductivity.

Magnetism of all samples is controlled by indirect RKKY interactions with the magnetic moments of Gd and Pr ordering antiparallel despite randomly occupying the same lattice site. Even though this has previously been assumed for mixed heavy and light lanthanide materials, this study shows direct evidence through XMCD at the Pr-L_2 and Gd-L_3 edges. Furthermore, XMCD shows the negative magnetization in samples with low Gd content to be a product of the differences in how the magnetic moments of different lanthanides develop with temperature. From here we demonstrate how weak negative and positive bias fields, applied during cooling, change the initial orientation of the Gd and Pr moments but maintain their antiparallel coupling over a wide range of temperatures, even when the measurement field, on heating, is replaced by a stronger opposing field. We further show how this can lead to magnetic compensation and magnetic memory effects as well as strong exchange bias in admixed, nearly compensated lanthanide systems with even minor local perturbations of commonly assumed fully random distribution of the lanthanide ions in the crystal lattice [55].

The data that support the findings of this study are available from the corresponding author upon reasonable request.

ACKNOWLEDGMENTS

This work was performed at Ames Laboratory and supported by the Materials Sciences and Engineering Division of the Office of Basic Energy Sciences, Office of Science of U. S. Department of Energy. Ames Laboratory is operated for the U.S. DOE by Iowa State University of Science and Technology under Contract No. DE-AC02-07CH11358. Use

of the Advanced Photon Source at Argonne National Laboratory was supported by the U.S. Department of Energy, Office of Science, Office of Basic Energy Sciences, under Contract No. DE-AC02-06CH11357. The authors would like to acknowledge the 11-BM staff at the Advanced Photon Source for performing the PXRD measurements.

T.D.R., A.K.P., and V.K.P. were responsible for conceptualization and design of the project. T.D.R., Y.M., and D.H. performed the data acquisition, analysis, and interpretation. T.D.R. drafted the manuscript. All authors contributed equally to the revisions of the manuscript.

The authors declare no competing interests

[1] M. Sagawa, S. Fujimura, N. Togawa, H. Yamamoto, and Y. Matsuura, New material for permanent magnets on a base of Nd and Fe, J. Appl. Phys. **55**, 2083 (1984).

[2] O. Gutfleisch, M. A. Willard, E. Brück, C. H. Chen, S. G. Sankar, and J. P. Liu, Magnetic materials and devices for the 21st century: Stronger, lighter, and more energy efficient, Adv. Mater. **23**, 821 (2011).

[3] V. K. Pecharsky and K. A. Gschneidner, Giant Magnetocaloric Effect in $Gd_5(Si_2Ge_2)$, Phys. Rev. Lett. **78**, 4494 (1997).

[4] S. Fujieda, A. Fujita, and K. Fukamichi, Large magnetocaloric effect in $La(Fe_xSi_{1-x})_{13}$ itinerant-electron metamagnetic compounds, Appl. Phys. Lett. **81**, 1276 (2002).

[5] Y. Li, G. Chen, W. Tong, L. Pi, J. Liu, Z. Yang, X. Wang, and Q. Zhang, Rare-Earth Triangular Lattice Spin Liquid: A Single-Crystal Study of $YbMgGaO_4$, Phys. Rev. Lett. **115**, 167203 (2015).

[6] Y. Tokiwa, M. Garst, P. Gegenwart, S. L. Bud'ko, and P. C. Canfield, Quantum Bicriticality in the Heavy-Fermion Metamagnet YbAgGe, Phys. Rev. Lett. **111**, 116401 (2013).

[7] A. P. Drozdov, P. P. Kong, V. S. Minkov, S. P. Besedin, M. A. Kuzovnikov, S. Mozaffari, L. Balicas, F. F. Balakirev, D. E. Graf, V. B. Prakapenka, E. Greenberg, D. A. Knyazev, M. Tkacz, and M. I. Eremets, Superconductivity at 250 K in Lanthanum Hydride under High Pressures, Nature (London) **569**, 528 (2019).

[8] T. Del Rose, A. K. Pathak, Y. Mudryk, and V. K. Pecharsky, Distinctive exchange bias and unusual memory effects in magnetically compensated $Pr_{0.75}Gd_{0.25}ScGe$, J. Mater. Chem. C **9**, 181 (2021).

[9] Y. Cao, S. Cao, W. Ren, Z. Feng, S. Yuan, B. Kang, B. Lu, and J. Zhang, Magnetization switching of rare earth orthochromite $CeCrO_3$, Appl. Phys. Lett. **104**, 232405 (2014).

[10] X. Zheng, P. Zheng, and R.-Z. Zhang, Machine learning material properties from the periodic table using convolutional neural networks, Chem. Sci. **9**, 8426 (2018).

[11] J. Schmidt, J. Shi, P. Borlido, L. Chen, S. Botti, and M. A. L. Marques, Predicting the thermodynamic stability of solids combining density functional theory and machine learning, Chem. Mater. **29**, 5090 (2017).

[12] Fifteen rare earths (R, excluding Sc and Pm), 27 transition metals (T, including Sc, excluding Y, La, and Tc), and 14 $3p$-$6p$ elements (X, excluding S, Po, halogens, and noble gases) result in 5670 possible RTX combinations.

[13] O. Janka, O. Niehaus, R. Pöttgen, and B. Chevalier, Cerium intermetallics with TiNiSi-type structure, Z. Naturforsch. B **71**, 737 (2016).

[14] R. Pöttgen and B. Chevalier, Equiatomic cerium intermetallics CeXX' with two p elements, Z. Naturforsch. B **70**, 695 (2015).

[15] H. Zhang and B.-G. Shen, Magnetocaloric effects in RTX intermetallic compounds (R = Gde-Tm, T = Fe-Cu and Pd, X = Al and Si), Chin. Phys. B **24**, 127504 (2015).

[16] A. Herrero, A. Oleaga, P. Manfrinetti, A. Provino, and A. Salazar, Study of the magnetocaloric effect in intermetallics RTX (R = Nd, Gd; T = Sc, Ti; X = Si, Ge), Intermetallics **110**, 106495 (2019).

[17] R. Pöttgen and B. Chevalier, Cerium intermetallics with ZrNiAl-type structure - A review, Z. Naturforsch. B **70**, 289 (2015).

[18] R. Pöttgen, O. Janka, and B. Chevalier, Cerium intermetallics CeTX - review III, Z. Naturforsch. B **71**, 165 (2016).

[19] S. Gupta and K. G. Suresh, Review on magnetic and related properties of RTX Compounds, J. Alloys Compd. **618**, 562 (2015).

[20] O. I. Bodak and Z. M. Kokhan, Issledovanie sistemy Ce - Sc - Ge, Izv. Akad. nauk SSSR. Neorg. Mater. **19**, 1094 (1983).

[21] P. Manfrinetti, A. V. Morozkin, O. Isnard, P. Henry, and A. Palenzona, Magnetic structure of the CeScSi-type RScGe Compounds (R = Pr, Nd, Tb), J. Alloys Compd. **450**, 86 (2008).

[22] F. Guillou, A. K. Pathak, T. A. Hackett, D. Paudyal, Y. Mudryk, and V. K. Pecharsky, Crystal, magnetic, calorimetric and electronic structure investigation of $GdScGe_{1-x}Sb_x$ Compounds, J. Phys.: Condens. Matter **29**, 485802 (2017).

[23] P. D. Kulkarni, U. V. Vaidya, S. K. Dhar, P. Manfrinetti, and A. K. Grover, New samarium and neodymium based admixed ferromagnets with near-zero net magnetization and tunable exchange bias field, J. Phys. D: Appl. Phys. **42**, 082001 (2009).

[24] A. K. Pathak, D. Paudyal, W. T. Jayasekara, S. Calder, A. Kreyssig, A. I. Goldman, K. A. Gschneidner, and V. K. Pecharsky, Unexpected magnetism, griffiths phase, and exchange bias in the mixed lanthanide $Pr_{0.6}Er_{0.4}Al_2$, Phys. Rev. B **89**, 224411 (2014).

[25] S. Singh, S. K. Dhar, P. Manfrinetti, A. Palenzona, and D. Mazzone, High Magnetic Transition Temperatures in RScT (R = Pr, Nd and Sm; T = Si and Ge) Compounds: Multiple Spin Reorientations in PrScGe, J. Magn. Magn. Mater. **269**, 113 (2004).

[26] T. Mahon, E. Gaudin, A. Villesuzanne, R. Decourt, J.-L. Bobet, O. Isnard, B. Chevalier, and S. Tencé, Hydrogen insertion in the intermetallic GdScGe: A drastic reduction of the dimensionality of the magnetic and transport properties, Inorg. Chem. **57**, 14230 (2018).

[27] S. Couillaud, E. Gaudin, V. Franco, A. Conde, R. Pöttgen, B. Heying, U. C. Rodewald, and B. Chevalier, The magnetocaloric properties of GdScSi and GdScGe, Intermetallics **19**, 1573 (2011).

[28] O. I. Bodak, Z. M. Shpyrka, and I. R. Mokra, Peculiarities of the Interaction of the Components in the Systems of Two Rare Earth Metals and Germanium, J. Alloys Compd. **247**, 217 (1997).

[29] A. P. Holm, V. K. Pecharsky, K. A. Gschneidner, R. Rink, and M. N. Jirmanus, X-ray powder diffractometer for in situ structural studies in magnetic fields from 0 to

35 kOe between 2.2 and 315 K, Rev. Sci. Instrum. **75**, 1081 (2004).

[30] B. H. Toby and R. B. von Dreele, GSAS-II: The genesis of a modern open-source all purpose crystallography software package, J. Appl. Crystallogr. **46**, 544 (2013).

[31] J. C. Lang and G. Srajer, Bragg transmission phase plates for the production of circularly polarized x rays, Rev. Sci. Instrum. **66**, 1540 (1995).

[32] M. Suzuki, N. Kawamura, M. Mizumaki, A. Urata, H. Maruyama, S. Goto, and T. Ishikawa, Helicity-modulation technique using diffractive phase retarder for measurements of x-ray magnetic circular dichroism, Jpn. J. Appl. Phys. **37**, L1488 (1998).

[33] See Supplemental Material at http://link.aps.org/supplemental/10.1103/PhysRevMaterials.6.044413 for synchrotron x-ray diffraction, SEM micrographs, and heat capacity data.

[34] P. Manfrinetti, M. Pani, A. Palenzona, S. K. Dhar, and S. Singh, Single crystal study of the high-curie-temperature ferromagnet $Gd_{1.02}Sc_{0.98}Ge$ and of $Gd_{2.38}Sc_{2.62}Ge_3$, J. Alloys Compd. **334**, 9 (2002).

[35] T. Mahon, E. Gaudin, A. Villesuzanne, B. Chevalier, and S. Tencé, Effect of carbon insertion on the structural and magnetic properties of NdScSi, Inorg. Chem. **58**, 15255 (2019).

[36] L. G. Dowell and A. P. Rinfret, Low-temperature forms of ice as studied by x-ray diffraction, Nature (London) **188**, 1144 (1960).

[37] Y. Mudryk, B. P. Alho, P. O. Ribeiro, and V. K. Pecharsky, Low-temperature crystal structure and mean-field modeling of $Er_xDy_{1-x}Al_2$ intermetallics, Metals **10**, 1662 (2020).

[38] Due to differences in measurement systems and sample preparations, the electrical conductivity used to calculate the electronic contribution to thermal conductivity is not the same $\rho(T)$ data displayed in Figs. 3(c) and 3(d), but rather p(T) data [displaying qualitatively the same behavior as shown in Figs. 3(c) and 3(d)] measured concurrently with thermal conductivity.

[39] B. Chevalier, H. Hermes, E. Gaudin, and R. Pottgen, New high temperature modification of CeTiGe: structural characterization and physical properties, J. Phys.: Condens. Matter **22**, 146003 (2010).

[40] S. Singh, S. K. Dhar, C. Mitra, P. Paulose, P. Manfrinetti, and A. Palenzona, The nature of magnetism in CeScSi and CeScGe, J. Phys. Condens. Matter **13**, 3753 (2001).

[41] M. A. Ruderman and C. Kittel, Indirect exchange coupling of nuclear magnetic moments by conduction electrons, Phys. Rev. **96**, 99 (1954).

[42] T. Kasuya, A theory of metallic ferro-and antiferromagnetism on zener's model, Prog. Theor. Phys. **16**, 45 (1956).

[43] K. Yosida, Magnetic proyerties of Cu-Mn alloys, Phys. Rev. **106**, 893 (1957).

[44] P. G. De Gennes, Interactions indirectes entre couches 4f dans les métaux de terres rares, J. Phys. Radium **23**, 510 (1962).

[45] W. M. Swift and W. E. Wallace, Magnetic characteristics of laves phase compounds containing two lanthanides with aluminum, J. Phys. Chem. Solids **29**, 2053 (1968).

[46] A. K. Pathak, D. Paudyal, Y. Mudryk, K. A. Gschneidner, and V. K. Pecharsky, Tunable Magnetism and Structural Transformations in Mixed Light- and Heavy-Lanthanide Dialuminides, Phys. Rev. B **94**, 224406 (2016).

[47] V. S. R. de Sousa, A. M. G. Carvalho, E. J. R. Plaza, B. P. Alho, J. C. G. Tedesco, A. A. Coelho, N. A. de Oliveira, and P. J. von Ranke, Investigation on the magnetocaloric effect in (Gd, Pr)A_{l2} solid solutions, J. Magn. Magn. Mater. **323**, 794 (2011).

[48] P. D. Kulkarni, S. Venkatesh, A. Thamizhavel, V. C. Rakhecha, S. Ramakrishnan, A. K. Grover, V. C. Rakhecham, S. Ramakrishnan, and A. K. Grover, Exchange bias and its phase reversal in zero magnetization admixed rare-earth intermetallics, IEEE Trans. Magn. **45**, 2902 (2009).

[49] P. D. Kulkarni, A. Thamizhavel, V. C. Rakhecha, A. K. Nigam, P. L. Paulose, S. Ramakrishnan, and A. K. Grover, Magnetic compensation phenomenon and the sign reversal in the exchange bias field in a single crystal of $Nd_{0.75}Ho_{0.25}Al_2$, Europhys. Lett. **86**, 47003 (2009).

[50] J. P. Rueff, R. M. Galé, S. Pizzini, A. Fontaine, L. M. Garcia, C. Giorgetti, E. Dartyge, and F. Baudelet, X-ray magnetic circular dichroism at the Gd L Edges in Gd-Ni-Co amorphous systems, Phys. Rev. B **55**, 3063 (1997).

[51] T. I. Ivanova, M. V. Gavrilko, S. A. Nikitin, I. A. Ovchenkova, A. V. Morozkin, D. Badurski, and K. P. Skokov, A magnetic and crystallographic study of new ternary $GdSc_xTi_{1-x}Ge$ compounds, J. Magn. Magn. Mater. **300**, e489 (2006).

[52] M. Buchner, K. Höfler, B. Henne, V. Ney, and A. Ney, Tutorial: Basic principles, limits of detection, and pitfalls of highly sensitive SQUID magnetometry for nanomagnetism and spintronics, J. Appl. Phys. **124**, 161101 (2018).

[53] A. K. Nayak, M. Nicklas, S. Chadov, C. Shekhar, Y. Skourski, J. Winterlik, and C. Felser, Large Zero-Field Cooled Exchange-Bias in Bulk Mn_2PtGa, Phys. Rev. Lett. **110**, 127204 (2013).

[54] R. Nirmala, A. V. Morozkin, A. K. Nigam, J. Lamsal, W. B. Yelon, O. Isnard, S. A. Granovsky, K. Kamala Bharathi, S. Quezado, and S. K. Malik, Competing magnetic interactions in the intermetallic compounds Pr_5Ge_3 and Nd_5Ge_3, J. Appl. Phys. **109**, 07A716 (2011).

[55] Y. Mudryk, D. Paudyal, V. K. Pecharsky, and K. A. Gschneidner, Low-temperature crystal structure and magnetic properties of Gd_5Ge_3, Phys. Rev. B **85**, 014116 (2012).